La$_{1-x}$Sr$_x$MnO$_3$ superlattices composed of ferromagnetic $x=0.4$ and antiferromagnetic $x=0.55$ layers

M. Izumi, T. Manako, and Y. Konishi

Joint Research Center for Atom Technology (JRCAT), Tsukuba 305-0046, Japan

M. Kawasaki

Joint Research Center for Atom Technology (JRCAT), Tsukuba 305-0046, Japan
and Department of Innovative and Engineered Materials, Tokyo Institute of Technology, Yokohama 226-8502, Japan

Y. Tokura

Joint Research Center for Atom Technology (JRCAT), Tsukuba 305-0046, Japan
and Department of Applied Physics, University of Tokyo, Tokyo 113-8656, Japan

A systematic study is presented for structural characterization and physical properties of La$_{1-x}$Sr$_x$MnO$_3$ ($x=0.4$, 0.55) single-layer films and superlattices composed of alternating stacks of these layers. By increasing the doping level from $x=0.4$ to $x=0.55$, the ground state of single-layer films is drastically changed from ferromagnetic to layered type antiferromagnetic with orbital ordering. The constituent layers in the superlattices appear to keep their ground states. Therefore the carriers are confined in the constituent layers, resulting in the modulation not only in spin but also in orbital structures along the stacking direction. Magnetoresistance is pronounced in the superlattices at low temperatures when the $x=0.55$ layer is very thin (e.g., $\leqslant 1.2$ nm), indicating restoration of the electronic coupling between the neighboring $x=0.4$ layers, which are otherwise decoupled by the $x=0.55$ layers.

I. INTRODUCTION

A wide variety of physical properties in perovskite manganese oxides is one of the current topics in materials science.[1] The physical properties of three-dimensional (3D) perovskite RE$_{1-x}$AE$_x$MnO$_3$, where RE is trivalent rare-earth element and AE is divalent alkaline-earth element, can be controlled easily by changing the average ion size of (RE, AE) site and doping level x. Among them, La$_{1-x}$Sr$_x$MnO$_3$ is a prototypical compound, which shows large magnetoresistance (MR) around the Curie temperature (T_C) for the doping level of the $0.15 \leqslant x \leqslant 0.5$.[2] The ferromagnetic (FM) transition takes place above 300 K at $0.3 \leqslant x \leqslant 0.5$.

The purpose of this paper is to investigate physical properties of FM/antiferromagnetic (AF) artificial oxide superlattices where FM layer is La$_{0.6}$Sr$_{0.4}$MnO$_3$. By combining the FM manganite layer with other perovskite compounds which have AF spin ordering in a form of superlattice, we can control the physical properties by utilizing the competition between FM and AF magnetic ordering structures in the constituent layers. Previously, we have reported the construction and the study on physical properties of the FM/AF superlattices composed of La$_{0.6}$Sr$_{0.4}$MnO$_3$ and La$_{0.6}$Sr$_{0.4}$FeO$_3$ having the same nominal doping level.[3] The AF La$_{0.6}$Sr$_{0.4}$FeO$_3$ has a G-type spin ordering and gives rise to spin frustration at the interface of the superlattices. The FM spin ordering in La$_{0.6}$Sr$_{0.4}$MnO$_3$ is modified to spin-canting in the vicinity of the interface by the proximity of the G-type AF spin arrangement, resulting in large MR at low temperatures due to the recovery of FM arrangement by the magnetic field. Similar results have also been reported with use of different combi-

nations of superlattice component.[4,5] In this paper, we present the preparation, structure, and magnetoelectronic properties of superlattice composed of Mn perovskites as a different type of FM/AF superlattices: FM La$_{0.6}$Sr$_{0.4}$MnO$_3$ ($x=0.4$) layer was combined with A-type AF La$_{0.45}$Sr$_{0.55}$MnO$_3$ ($x=0.55$) layer having the $d_{x^2-y^2}$ orbital ordering.

Unlike Pr$_{1-x}$Sr$_x$MnO$_3$ (Ref. 6) or Nd$_{1-x}$Sr$_x$MnO$_3$,[7] La$_{1-x}$Sr$_x$MnO$_3$ is free from charge ordering phenomenon even when $x=0.50$, but changes its ground state to an AF metal at $x>0.5$.[8] Physical properties of the AF compounds with high doping level have been studied only using polycrystalline samples because of difficulty in the fabrication of a bulk single crystal. An alternative approach to fabricate well defined single crystals suitable for physical research is to synthesize high quality epitaxial thin films.[9–11] Occasionally, it is possible to make single crystalline film specimen for the materials which cannot be grown as bulk single crystals. In the case of epitaxial thin films, however, the strain effect caused by the lattice mismatch from the substrate has to be taken into account.[12–16]

Recently, we have investigated the structures and properties of single crystalline La$_{1-x}$Sr$_x$MnO$_3$ thin films grown on various substrates. The coherent strain from the substrate can stabilize various ground states even in case the composition is fixed. For example, in the case of La$_{0.5}$Sr$_{0.5}$MnO$_3$ films grown on lattice mismatched substrates, the lattice anisotropy c/a of the films can be controlled to a considerable extent, e.g., from 0.976 on SrTiO$_3$ through 0.994 on [(LaAlO$_3$)$_{0.3}$-(SrAl$_{0.5}$Ta$_{0.5}$O$_3$)$_{0.7}$] to 1.041 on LaAlO$_3$, where a and c are the lattice parameters of the films along

　　　　　　PRB **61**　　12 187

[100] and [001] directions in the tetragonal symmetry, respectively. As the crystal is tetragonally distorted, the ground state was drastically changed from layered type (A-type) AF to chain type (C-type) AF by way of the conventional FM state near $c/a = 1$. A theoretical study on the electronic and magnetic structure using density-functional calculation[17] could quantitatively reproduce the experimental phase diagram that is drawn on the plane of the hole doping x vs the lattice strain c/a. According to the calculation, the orbital ordering of $d_{x^2-y^2}$ is stabilized for $c/a < 1$, while that of $d_{3z^2-r^2}$ for $c/a > 1$, accompanying the A-type and the C-type AF spin structure, respectively. This technique to stabilize various ground states may be applied to a wide variety of research such as investigation of physical properties on well defined single crystalline films, surface characterization in terms of electronic and magnetic properties, strain effect induced by lattice mismatched substrates, and devices based on heterostructures. Among them, the magnetic and electronic property at the surface or the interface in the oxide systems is a challenging issue, and the present study is one such approach. The aforementioned complex properties are the consequence of collective phenomena played by strongly correlated electrons of which ground states are sensitive to lattice structure, orbital structure, doping level, and magnetic interaction. Therefore large modification of properties is anticipated to take place in the vicinity of the interface.

First, the $x = 0.55$ films grown on SrTiO$_3$ substrates were characterized so as to establish the magnetic, electronic, and structural basis of the superlattice research. Structure and magnetic properties of the superlattices are characterized to show that the constituent layers keep their ground states with atomically abrupt interface in magnetic ordering. Nevertheless, transport properties highlight the importance of orbital mixing at the interface and spin canting in A-type AF layers upon application of a magnetic field, both of which lead an enhanced electron hopping along the c axis in the A-type AF layers otherwise acting as barriers for carrier motion.

II. EXPERIMENT

La$_{1-x}$Sr$_x$MnO$_3$ ($x = 0.4$, 0.55) single-layer films (100 nm thick) and $x = 0.4/x = 0.55$ superlattices were fabricated by using a pulsed laser deposition method employing stoichiometric targets as reported previously.[18] For achieving atomically regulated epitaxy, SrTiO$_3$ (001) single-crystal substrates treated with NH$_4$F-HF solution were used.[19] Prior to the deposition, the substrate was *in situ* annealed at 900 °C in 1 mTorr of oxygen for 20–30 min, resulting in the well defined TiO$_2$ terminated surface having straight and evenly aligned steps apart by about 150 nm (corresponding to a miscut angle of 0.15°). After the procedure, the film deposition was carried out at a substrate temperature of 800 °C while keeping 1 mTorr oxygen pressure. KrF excimer laser pulses of 100 mJ were focused on a target at a fluence of 3 J/cm^2. During the deposition, reflection high-energy electron diffraction (RHEED) pattern was monitored by a charge-coupled device camera and real-time analyses were carried out by a computer. We could routinely observe persisting oscillation of specular beam intensity.[3,14] By counting the RHEED oscillation, the thicknesses of $x = 0.4$ and x

$= 0.55$ layers in the superlattices were regulated on an atomic scale.

After the deposition, the films were cooled in 760 Torr of oxygen. In the inspection by an atomic force microscope, the superlattices showed a step-and-terrace structure similar to that of the substrate, indicating that the film was grown in an almost ideal two-dimensional (2D) layer-by-layer growth mode. X-ray diffraction (XRD) was carried out by a four-circle diffractometer with CuKα source. In conventional 2θ-θ scan with the scattering vector perpendicular to the film plane, no peak was observed other than intended (00l) peaks and satellite peaks associated with superlattices structure. Reciprocal space mapping was also carried out for superlattices as well as single-layer films. Magnetization was measured by a superconducting quantum interference device magnetometer. Magnetic field was applied parallel to the film plane to avoid the geometric demagnetization effect. Resistivity with magnetic field up to 7 T applied along the film plane was measured by a four-probe method.

III. RESULTS AND DISCUSSION

A. Magnetic properties of La$_{1-x}$Sr$_x$MnO$_3$ single-layer films

Magnetization and resistivity of La$_{1-x}$Sr$_x$MnO$_3$ ($x = 0.40$, 0.55) single-layer films with thickness of 100 nm are shown in Fig. 1. The $x = 0.4$ film shows FM transition at $T_C = 330$–340 K and saturation magnetization of 3.5μ_B/Mn at 5 K corresponding to the full magnetic moment. Large negative MR is observed around T_C which is well known as dominated by the double-exchange mechanism.[2] The reduced T_C compared with 370 K for the bulk crystal is due to the epitaxial strain of lattice as reported previously.[14] The lattice parameters determined from the reciprocal space mapping for single-layer films are listed in Table I. The in-plane lattice parameters a for the both films are expanded so as to match with that of the substrate. As a result, the out-of-plane lattice parameters c are elastically deformed. Such a coherent strain can be observed even for 100-nm-thick films when the substrate surface structure and the deposition conditions are well optimized as in the present study.

With increasing the hole doping level to $x = 0.55$, the ground state is changed to an AF metal. AF transition was observed at a Néel temperature (T_N) of 220–230 K, as seen as a broad cusp in Fig. 1(a). The transport property stays barely metallic and negative MR remains at low temperatures. The MR defined as $[\rho(0\ T) - \rho(7\ T)]/\rho(7\ T)$ is as large as 23% even at 5 K. By the analogy to the features observed for bulk La$_{1-x}$Sr$_x$MnO$_3$ (Ref. 8) and Nd$_{1-x}$Sr$_x$MnO$_3$ (Ref. 20–22) crystals ($x > 0.5$) as detailed in the following, we attribute the ground state to the A-type antiferromagnetism as depicted in the inset of Fig. 1(a). In the A-type spin structure, magnetic moment is ordered ferromagnetically in the ab plane of MnO$_2$ layers and these layers are antiferromagnetically coupled along the c direction.

It is known for the bulk crystals of perovskite manganese oxides that increasing of the doping level above $x = 0.5$ tends to stabilize the AF state. In the case of La$_{1-x}$Sr$_x$MnO$_3$ and Nd$_{1-x}$Sr$_x$MnO$_3$ system, for example, the compounds with $0.5 < x < 0.6$ show the AF and metallic ground state without charge ordering.[8,20–22] The appearance of this interesting phase can be explained in terms of subtle competition and
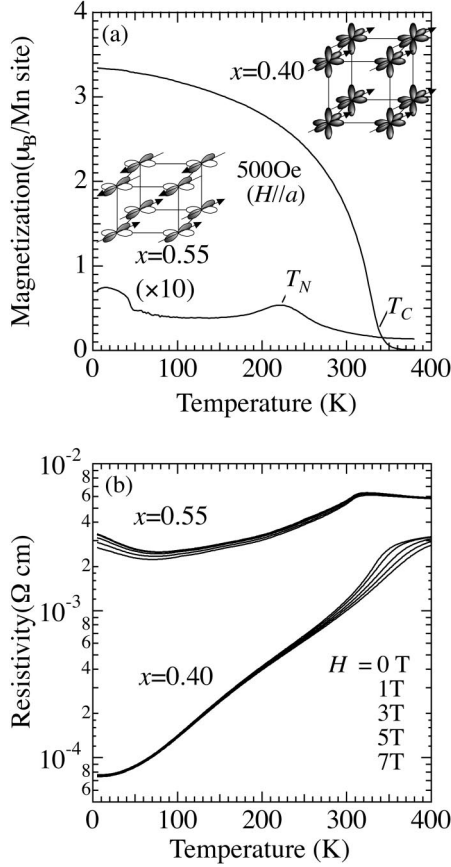
FIG. 1. Magnetic and electrical properties of 100-nm-thick La$_{1-x}$Sr$_x$MnO$_3$ ($x=0.4$ and 0.55) single-layer films grown on SrTiO$_3$ (001) substrate. (a) Temperature dependence of magnetization measured during cooling in a magnetic field of 500 Oe (FC) applied along the [100] direction in the film plane. Ferromagnetic and antiferromagnetic transitions were observed at T_C $=330$–340 K and $T_N=220$–230 K, respectively. (b) Temperature dependence of resistivity measured during cooling in various magnetic fields. Magnetic fields were applied parallel to the current in the film plane. The inset to (a) is the spin and orbital structures: The $x=0.4$ film has ferromagnetically ordered spins with disordered orbitals, while the $x=0.55$ film is A-type antiferromagnetic spins with ordered $d_{x^2-y^2}$ orbitals.

compromise between the double-exchange interaction mediated with the carrier e_g electron and the t_{2g} spin superexchange interaction. Namely, the $d_{x^2-y^2}$-type orbital is ordered in the ab plane to maximize the carrier kinetic energy via the double exchange interaction, yet spins are coupled antiferromagnetically along the c axis to gain the superexchange energy. This intuitive scenario has in fact been substantiated by several theoretical calculations.[23–26] Upon the phase transition to the layer-type (A-type) spin ordering as-

sociated with such orbital ordering, the bulk crystal shows the spontaneous macroscopic strain, i.e., the expansion of the ab-plane lattice parameters and the shrinkage of the c-axis parameter, due to coupling of the ordered orbital with the cooperative Jahn-Teller distortion.[20,21] This antiferromagnet is in sharp contrast to the $d_{x^2-y^2}/d_{3z^2-r^2}$ quantum-disordered orbital structure in the FM-metallic state, as realized in the present $x=0.4$ film, and also to the A-type but insulating state with alternate $d_{3x^2-r^2}/d_{3y^2-r^2}$ ordering in LaMnO$_3$.[27,28]

Our assignment of the observed AF metallic state of the $x=0.55$ film to the A-type state with $d_{x^2-y^2}$ orbital ordering is based on the following features of the present epitaxial film. First, the composition ($x=0.55$) is in the regime of the overdoping that diminishes the double-exchange interaction and relatively stabilize the superexchange interaction as observed for the corresponding bulk crystals. More importantly, the presence of the macroscopic biaxial strain in the present $x=0.55$ thin film, expressed as a small c/a value (0.970) as shown in Table I, can further favor such an orbital-ordered A-type state. Conversely, the external biaxial strain should stabilize the A-type AF spin ordered state via the Jahn-Teller channel rather than the FM state with orbital disordered state.

B. A-site modulated La$_{1-x}$Sr$_x$MnO$_3$ superlattice

1. Structural characterization

We have fabricated numbers of $[x=0.4$ (m u.c.)/x $=0.55$ (n u.c.)]$_{20}$ (u.c. stands for unit cells) superlattices on SrTiO$_3$ substrates. Hereafter, we express the combination of layer thicknesses in superlattices as $[F_m, A_n]$, where F and A represents the $x=0.4$ (FM) and $x=0.55$ (AF) layers, respectively. As discussed in the previous section, the anisotropy of crystal structure represented as c/a plays an important role in defining the ground state. When we construct superlattices composed of A-type AF and FM layers, not only the composition but also the crystal structure is modulated alternately along the growth direction, both of which should give rise to XRD satellite peaks.

Figure 2 exemplifies a contour mapping of reciprocal lattice around (114) peak of a $[F_{10}, A_3]$ superlattice measured by using a four-circle diffractometer. Horizontal and vertical axes are Q vectors in the reciprocal lattice along the [110] direction (in-plane) and [001] direction (out-of-plane), respectively. Near the (114) peak of the substrate, there can be seen a sharp and strong peak denoted as 0, corresponding to the fundamental Bragg diffraction of perovskite. The Q_{110} value of the superlattice is identical to that of the substrate, indicating coherently strained epitaxy of the superlattice. Namely, there is no misfit dislocation at the interfaces be-

TABLE I. Lattice parameters and crystal symmetry of the $x=0.4$ and 0.55 single-layer films of La$_{1-x}$Sr$_x$MnO$_3$ together with those of the SrTiO$_3$ substrate.

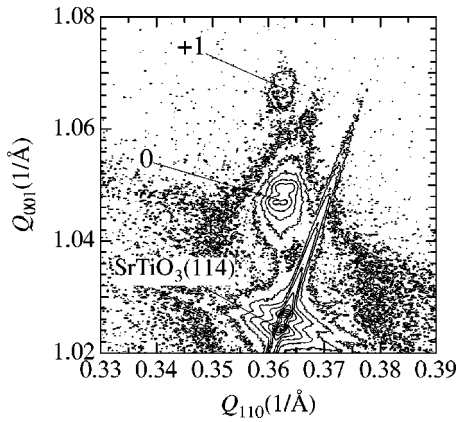|	Symmetry	a(nm)	c(nm)	c/a
$x=0.4$	tetragonal	0.391	0.384	0.983
$x=0.55$	tetragonal	0.391	0.379	0.970
SrTiO$_3$	cubic	0.3905	0.3905	1

FIG. 2. Reciprocal lattice mapping of x-ray diffraction around the perovskite (114) peak for a $[x=0.4$ (10 u.c.)$/x=0.55$ (3 u.c.)$]_{20}$ superlattice. The horizontal and vertical axes are along [110] and [001] directions, respectively. Doublet peaks are due to $K\alpha_1$ and $K\alpha_2$ of Cu radiation. Fundamental peak and superlattice peak denoted as 0 and $+1$, respectively, are observed at the same Q_{110} values as that of the substrate, indicating the coherent epitaxy of the superlattice film.

tween the adjacent constituent layers as well as at the interface between the film and the substrate.

The satellite peak denoted as $+1$ in Fig. 2 originates from superlattice modulation along the growth direction. To analyze the superstructure along the growth direction, 2θ-θ scan was performed for the same $[F_{10}, A_3]$ superlattice as shown for the (001) and (003) zone areas in Fig. 3. Although satellite peaks can be seen in the both areas, we note the fact that the intensity of satellite peak is asymmetric around fundamental peak around the (001) fundamental peak. This large asymmetry can be explained only when we take account of the c-lattice parameter modulation and the compositional modulation between constituent layers as discussed below. We have carried out the simulation of the satellite peaks based on the one-dimensional step model.[29,30] We examined the following four models, as also depicted in the lower panel of Fig. 3, by the combinations of the two factors, i.e., the composition and the c-axis lattice parameter.

(i) La/Sr concentration modulation is completely smeared out (diffused) to yield an averaged Sr content of $x=0.435$ and therefore the lattice parameter c shows an averaged value of 0.383 nm.

(ii) La/Sr concentration has perfect modulation as designed. However, the lattice parameter c yields an averaged value of 0.383 nm.

(iii) La/Sr concentration is completely diffused. However, the lattice parameter c is perfectly modulated as 0.384 and 0.379 nm. (Although it is hard to rationalize this case, this calculation highlights the importance of lattice modulation for the appearance of satellite peaks.)

(iv) La/Sr concentration is ideally abrupt at the interface and the lattice parameter c is also perfectly modulated. This model stands for the ideal case.

The calculated peak position and the relative intensity normalized by that of the fundamental perovskite peak are plotted in Fig. 3. The experimental result well agrees with the model (iv) where both La/Sr composition and lattice parameter c are ideally modulated: The observed satellite peak
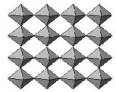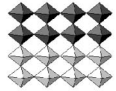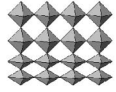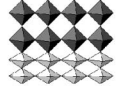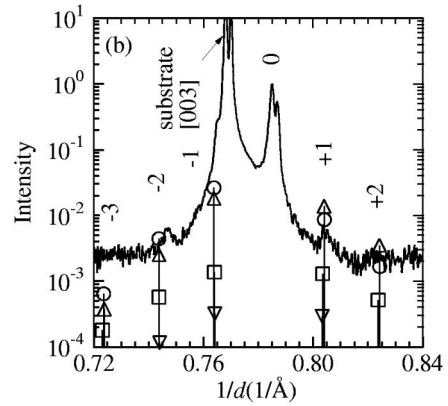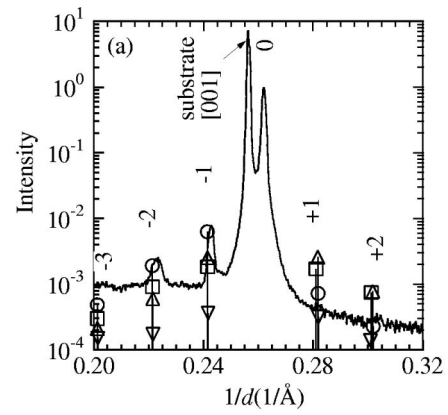

Model		composition	c-axis length
(I)		diffused $La_{1-x}Sr_xMnO_3$ ($x=0.4346$)	averaged value 3.828Å
(II)		modulated $La_{0.6}Sr_{0.4}MnO_3$ $+La_{0.45}Sr_{0.55}MnO_3$	averaged value 3.828Å
(III)		diffused $La_{1-x}Sr_xMnO_3$ ($x=0.4346$)	modulated 3.840Å($x=0.40$) $+3.786$Å($x=0.55$)
(IV)		modulated $La_{0.6}Sr_{0.4}MnO_3$ $+La_{0.45}Sr_{0.55}MnO_3$	modulated 3.840Å($x=0.40$) $+3.786$Å($x=0.55$)

FIG. 3. 2θ-θ scan of x-ray diffraction around (a) (001) and (b) (003) fundamental peaks for a $[x=0.4$ (10 u.c.)$/x=0.55$ (3 u.c.)$]_{20}$ superlattice. The numbers denoted on the peaks indicate the nth superlattice peak. The peak intensities of satellite peaks are normalized by the those of perovskite fundamental peak denoted as 0. Intensities of satellite peaks are calculated with the one-dimensional step model by assuming the four models with different modulation structures in La/Sr composition and lattice parameter as illustrated in the lower panel (see also text).

position and asymmetric peak profile, in which intensity of satellite peaks in the left side of the fundamental peak are 20 times as high as those in the right side, are quantitatively reproduced. Even when either of modulations in the lattice
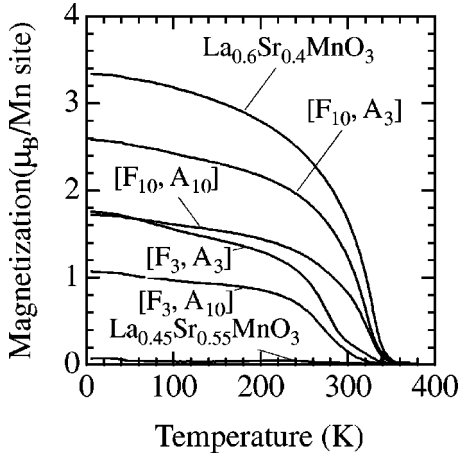
FIG. 4. Temperature dependence of magnetization for the x $=0.4/x=0.55$ superlattices measured during cooling in a magnetic field of 500 Oe applied along [100] in the film plane and normalized by the total number of Mn ions in the superlattices. The respective layer thickness of the constituent $x=0.4$ (F) and $x=0.55$ (A) layers is given by m unit cells and n unit cells in the notation of $[F_m, A_n]$, respectively. The data for the $x=0.4$ and $x=0.55$ single-layer films are also shown for comparison.

parameter c or the La/Sr compositional modulation is missing, the peak profile cannot be reproduced as seen in Fig. 3. Therefore even the $x=0.55$ layer is as thin as 3 u.c. in the superlattice, the large tetragonal distortion c/a is kept as that of the thick $x=0.55$ single-layer film, suggesting that A-type AF spin ordering is stabilized via $d_{x^2-y^2}$ orbital ordering. This result gives an important conjecture on the carrier dynamics in the superlattice: The carriers in the respective constituent layers will be well confined due to the persistent A-type AF spin ordering as well as to the persistent $d_{x^2-y^2}$ orbital ordering in the $x=0.55$ layer. This will be argued in the latter subsection in detail.

2. Magnetization

Figure 4 shows magnetization of the superlattices as a function of temperature. The magnetization is normalized by the total number of the Mn ion in the superlattices. All the superlattices show a clear FM transition. T_C is scarcely changed by the $x=0.4$ layer thickness. Even when the x $=0.4$ layer is as thin as 3 u.c. (1.2 nm), T_C remains as high as 280–290 K. To estimate the absolute value of magnetization, M-H curves were measured at 5 K, as shown in Fig. 5. In the both processes after zero field cooling (ZFC) and after field cooling (FC), hysteresis loops showed almost the same saturation magnetization, remanent magnetization, and coercive force (H_C). Except for slight difference in H_C of the respective superlattices, no significant change depending on the layer thickness was observed in hysteresis curves. This result indicates that spin canting arising from magnetic coupling at the interface between FM and AF layers is minimal in this type superlattice. Figure 6 shows variation of the remanent magnetization obtained from the hysteresis loops measured at 5 K after ZFC. The magnetization appears to be simply proportional to the volume fraction of the $x=0.4$ layer, $t_{0.4}/(t_{0.4}+t_{0.55})$, where $t_{0.4}$ and $t_{0.55}$ are layer thickness for the $x=0.4$ and the $x=0.55$ layers, respectively. In other
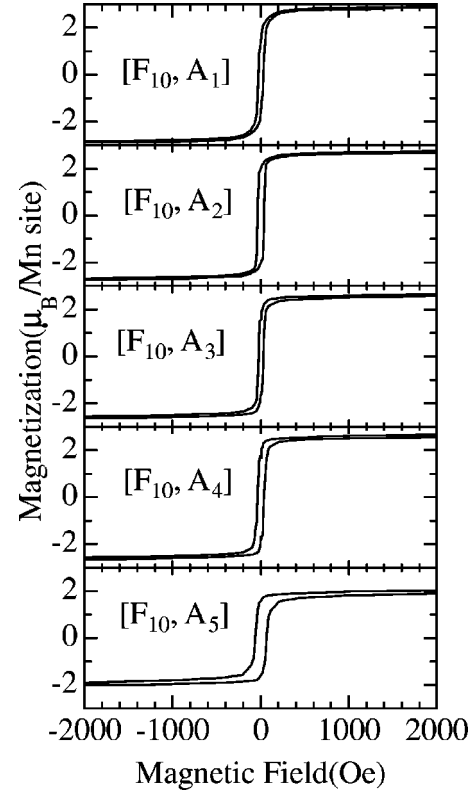

FIG. 5. Magnetic-field dependence for the magnetization of x $=0.4/x=0.55$ superlattices. The $x=0.4$ (F) layer thickness is fixed to be 10 unit cells (u.c.) while the $x=0.55$ (A) layer thickness is varied from 1 to 5 u.c. The values of magnetization are normalized by the total number of Mn ions in the superlattices. The hysteresis curve was measured after the zero field cooling and magnetic field was applied along the a axis. There is no difference between the hysteresis shapes after zero field cooling and after field cooling.

words, it appears that the observed magnetization comes from the $x=0.4$ layers alone, and that the $x=0.55$ layers have the same AF state to that of the single-layer film. This assignment is consistent with the aforementioned results of
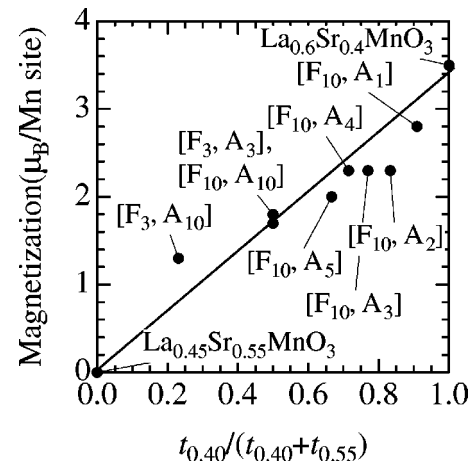

FIG. 6. Remanent magnetization at 5 K normalized by the total number of Mn ions is plotted as a function of volume fraction of the FM layers, $t_{0.4}/(t_{0.4}+t_{0.55})$, where $t_{0.4}$ and $t_{0.55}$ represent the thicknesses of the $x=0.4$ and the $x=0.55$ layers, respectively.

the structural characterization: c/a of the $La_{0.45}Sr_{0.55}MnO_3$ layer is kept anisotropic even in the superlattices, perhaps reflecting the $d_{x^2-y^2}$-type orbital ordering and A-type AF ordering. Therefore we conclude that spin and orbital structures are modulated in the $x=0.4/x=0.55$ superlattices with abrupt interface on an atomic scale.

Even though orbital and spin structures are dramatically different, the $x=0.4$ and $x=0.55$ layers appear to maintain their structure and physical properties in the superlattices. This is in striking contrast to the previously reported FM/AF superlattices.[3] The ferromagnetism of $La_{0.6}Sr_{0.4}MnO_3$ is strongly suppressed by combining with G-type AF $La_{0.6}Sr_{0.4}FeO_3$ in the superlattice. When 10-u.c.-thick $La_{0.6}Sr_{0.4}MnO_3$ is combined with a 5-u.c.-thick $La_{0.6}Sr_{0.4}FeO_3$ layer, T_C and magnetization of the $La_{0.6}Sr_{0.4}MnO_3$ layer are suppressed to 185 K and $0.8\mu_B$, respectively, and the ferromagnetism disappears for the 5-u.c.-thick $La_{0.6}Sr_{0.4}MnO_3$ layer. Such remarkable suppression of the FM state adjacent to the G-type AF state can be explained by the presence of spin frustration at the interface. In the case of G-type AF spin ordering, (001) plane shows a staggered pattern of the spin arrangement, and hence causes the spin frustration at the interface with the FM layer in the presence of the exchange interaction between the Mn and Fe spins. This induces appreciable spin canting and critically suppresses ferromagnetism of $La_{0.6}Sr_{0.4}MnO_3$. On the contrary, such a spin frustration does not exist at the FM/A-type AF interface in the present superlattice, since spins of the A-type AF state are ordered ferromagnetically on the (001) interface plane. Ferromagnetism of the $x=0.4$ layer is hardly modified in this type of superlattices, and hence the variation of spin ordering structure can be abrupt on an atomic scale.

To understand the magnetic properties of the superlattices, magnetic coupling between FM and A-type AF layers has to be considered. Figure 7 shows possible configurations of magnetic ordering structure. If there is distinct ferromagnetic or antiferromagnetic coupling between neighboring FM and AF layers as shown in Fig. 7(a), the coupling between the neighboring FM layers should depend on whether the number of intervening AF atomic layers is even or odd; even atomic layers of AF induces antiferromagnetic coupling between adjacent FM layers and odd atomic layers of AF does ferromagnetic coupling. In the former case, the remanent magnetization should apparently disappear even though the respective FM layer shows full magnetic moment. In our experiment, however, there can be seen no such an even-odd effect (see and compare, for example, $[F_{10}, A_n]$ ($n = 1, 2, 3, 4,$ and 5) superlattices in Figs. 5 and 6). Therefore, we can conclude that the interface of the present FM/AF superlattice probably takes the 90° magnetic coupling as depicted in Fig. 7(b). Such a 90° magnetic coupling is observed in the Fe films grown on stepped Cr (001) substrate,[31,32] in which the net magnetic moment is directed perpendicular to the magnetic easy axis of AF layer even in the case of collinear magnetic coupling between neighboring spins at the FM/AF interface.[33]

3. Resistivity

Figure 8 shows the resistivity in magnetic fields for superlattices where layer thickness and combination are

AF layer thickness	even	odd
(a) FM coupling*	FM / AF / FM	FM / AF / FM
(b) 90° rotation	FM / AF / FM	FM / AF / FM
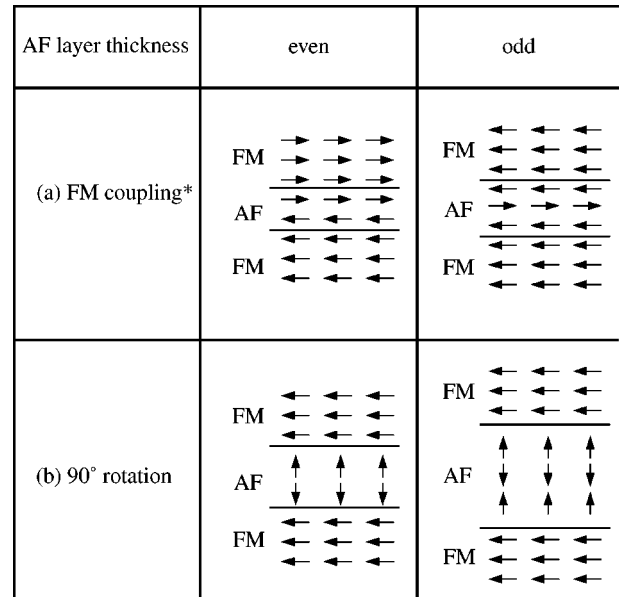
* AF inter-layer coupling gives the same apparent magnetization

FIG. 7. Possible spin arrangements at the interface. (a) Magnetic coupling at the interface between FM and A-type AF layers is ferromagnetic. In zero field, the magnetic coupling between adjacent FM layer depends on whether the number (even or odd) of atomic layers in the AF layer. (b) The relative spin angle between FM and AF layer is 90°. There is no magnetic coupling between adjacent FM layers.

$[F_3, A_3]$, $[F_3, A_{10}]$, $[F_{10}, A_3]$, and $[F_{10}, A_{10}]$. The resistivity was calculated with taking the total superlattice thickness into account. At a glance, it is noticeable that the resistivity and MR behaviors are similar to each other regardless of the combination. All the superlattices show metallic temperature dependence of resistivity. Although the magnitude depends on the combination, negative MR was observed over a whole temperature region. When we com-
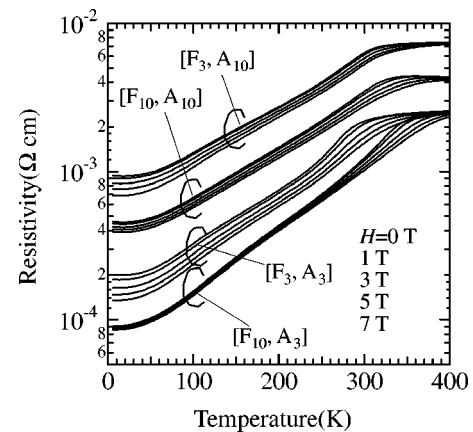
FIG. 8. Temperature dependence of resistivity for $[F_3, A_3]$, $[F_3, A_{10}]$, $[F_{10}, A_3]$, and $[F_{10}, A_{10}]$ superlattices in magnetic fields. m and n in the notation of $[F_m, A_n]$ represent the number of unit cells (u.c.) of the constituent ferromagnetic (F) $x=0.4$ and antiferromagnetic (A) $x=0.55$ layers of the superlattices involving 20 repeat units, respectively. The resistivity was measured with decreasing temperature. Magnetic field was applied parallel to the current direction within the film plane.

pare the resistivity between superlattices having the same x =0.4 layer thickness, such as $[F_3,\ A_3]$ vs $[F_3,\ A_{10}]$ and $[F_{10},\ A_3]$ vs $[F_{10},\ A_{10}]$, the resistivity increases with increasing the x=0.55 layer thickness.

Before going to discussion on the superlattice, let us show first review the transport characteristics of the A-type AF single layer. The resistivity of the A-type AF x=0.55 single layer is higher than that of the 3D ferromagnet, i.e., x=0.4 layer, as seen in Fig. 1(b). In the ground state of the A-type antiferromagnet, conduction electrons can move only in the ab plane, and cannot hop between adjacent MnO$_2$ layers because of the AF coupling along c direction. An important consequence of the A-type spin ordering is a huge anisotropy of charge dynamics. According to the double-exchange model, electron hopping is expressed as

$$t=t_0\cdot\cos(\theta/2), \qquad (1)$$

where θ is the relative angle between the spins on adjacent sites.[34] Therefore the c-axis AF coupling (θ=180°) in the A-type state may confine the carrier motion within the FM ab plane. A huge anisotropy of the c axis to the ab-plane resistivity (amounting to 10^4) as observed for a single crystal of Nd$_{1-x}$Sr$_x$MnO$_3$ (x=0.55) has confirmed such a 2D metallic state in the A-type AF state.[21]

The results of structural characterization and magnetization measurement on the superlattices indicate that the x =0.4 and the x=0.55 layers keep original FM and A-type AF properties, respectively. Considering the 2D nature of carrier dynamics in the A-type layer, the resistivity of the superlattices can be regarded to the first approximation as a parallel circuit of component layers. On this ground, the ground-state (5 K) conductivity (σ) of the superlattices is plotted against the volume fraction of the x=0.4 layers, $t_{0.4}/(t_{0.4}+t_{0.55})$, in Fig. 9. The parallel-circuit model can explain, as in the case of magnetization results, overall transport properties qualitatively. For example, when the intervening AF (x=0.55) layer thickness is as large as 10 u.c., σ of the superlattice appears to be simply proportional to the volume fraction of the constituent x=0.4 films, as represented by a broken line in Fig. 9. In a simple parallel-circuit model, σ of superlattice is expressed as

$$\sigma=\sigma_{0.4}\times t_{0.4}/(t_{0.4}+t_{0.55})+\sigma_{0.55}\times t_{0.55}/(t_{0.4}+t_{0.55}), \quad (2)$$

where $\sigma_{0.4}$ and $\sigma_{0.55}$ are the conductivity of x=0.4 and x =0.55 layers in the superlattices, respectively. However, when the thickness of the constituent x=0.55 layers is small enough ($\leqslant$5 u.c.), the superlattice cannot be considered as a parallel circuit. As indicated by a solid line in Fig. 9, the superlattice with $[F_{10},\ A_n](n\leqslant5)$ shows much higher σ than the extrapolated value (a broken line) of the n=10 based parallel-circuit model. As a clear example, $[F_3,\ A_3]$ and $[F_{10},\ A_{10}]$ superlattices, both having the FM layers with 50% volume fraction, show quite a different behavior of σ (a broken arrow in Fig. 9). The σ of $[F_3,\ A_3]$ superlattice, 5000 Ω^{-1} cm^{-1}, is twice as large as that of $[F_{10},\ A_{10}]$ superlattice, 2200 Ω^{-1} cm^{-1} at 5 K, in spite of higher T_C of $[F_{10},\ A_{10}]$ than that of $[F_3,\ A_3]$ (see Fig. 4). This indicates that we may have to consider the mixing of spin-orbital structure between the two constituent layers at the interface.
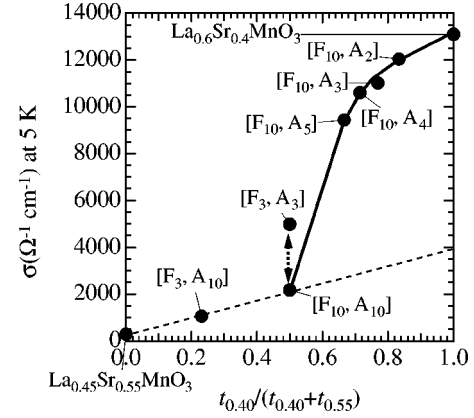

FIG. 9. Conductivity σ at 5 K as a function of volume fraction $t_{0.4}/(t_{0.4}+t_{0.55})$, where $t_{0.4}$ and $t_{0.55}$ represent the thicknesses of the constituent x=0.4 and x=0.55 layers, respectively. σ is normalized by the total thickness of the superlattice. The σ values of the x =0.4 and the x=0.55 100-nm-thick single-layer films are shown for the comparison. A solid line represents a relationship between $t_{0.4}/(t_{0.4}+t_{0.55})$ and σ of the x=0.4 single-layer film or the superlattices whose x=0.4 layer thickness is fixed to be 10 u.c. A broken line connects the data of the x=0.55 single-layer film and the superlattices whose x=0.55 layer thickness is fixed to be 10 u.c. The intersection between the broken line and the right ordinate may indicate σ of a hypothetical La$_{0.6}$Sr$_{0.4}$MnO$_3$ single layer where thickness is thin enough ($\leqslant$10 u.c.). Two superlattices of $[F_3,\ A_3]$ and $[F_{10},\ A_{10}]$, having the same $t_{0.4}/(t_{0.4}+t_{0.55})$, show different σ as indicated by the broken arrow.

To elucidate the carrier motion at the interface, we argue the transport properties in a magnetic field. Magnetic field increases σ monotonically and the magnetoconductivity $[\sigma(H)-\sigma(0)]$ is in near proportion with magnetic field (not shown). Figure 10 shows the temperature dependence of magnetoconductivity, $\Delta\sigma=\sigma(7\ \text{T})-\sigma(1\ \text{T})$, for the superlattices and the single-layer films (note a logarithmic scale on the ordinate). The $\Delta\sigma$ can be expressed to the first approximation from Eq. (2) as

$$\Delta\sigma=\Delta\sigma_{0.4}\times t_{0.4}/(t_{0.4}+t_{0.55})+\Delta\sigma_{0.55}\times t_{0.55}/(t_{0.4}+t_{0.55}), \tag{3}$$
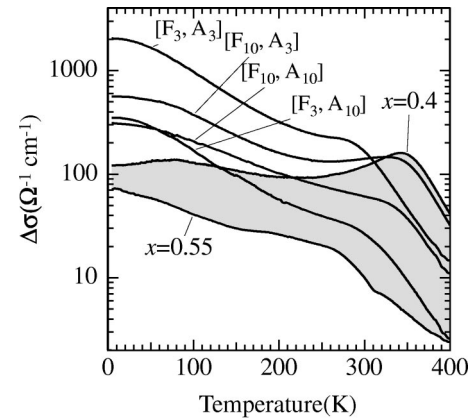

FIG. 10. Temperature dependence of magnetoconductivity $\Delta\sigma$, $[\sigma(7\ \text{T})-\sigma(1\ \text{T})]$, of the respective superlattices. $\Delta\sigma$ of the x=0.4 and the x=0.55 single-layer films are shown for comparison. A shaded area indicates the region which is represented by the parallel-circuit model (see text).

where $\Delta\sigma_{0.4}$ and $\Delta\sigma_{0.55}$ are the magnetoconductivity of $x = 0.4$ and $x = 0.55$ layers in the superlattices, respectively. In this model, $\Delta\sigma$ in the superlattice should position between the $\Delta\sigma$ curves for the $x = 0.4$ and the $x = 0.55$ single-layer films, as indicated by a hatched area in Fig. 10. In Fig. 10, $\Delta\sigma$ has a peak around T_C and increases further toward low temperature. The peak of $\Delta\sigma$ around T_C arises from the first term in Eq. (3), i.e., conventional MR effect of the FM $x = 0.4$ layer. The magnitude of $\Delta\sigma$ at T_C is reasonable (within the shaded area in Fig. 10) when the volume fraction of the FM layers is taken into account. However, $\Delta\sigma$ of the superlattices at low temperatures is much larger than those for single-layer films and rather enhanced *with decreasing* the $x = 0.55$ layer thickness. For example, $\Delta\sigma$ of $[F_3, A_3]$ superlattice at 5 K is as large as 2000 Ω^{-1} cm^{-1} and much larger than those of $x = 0.55$ (70 Ω^{-1} cm^{-1}) and $x = 0.4$ (120 Ω^{-1} cm^{-1}). Therefore $\Delta\sigma$ in superlattices at low temperatures cannot be explained well by the simple parallel-circuit model when the constituent $x = 0.55$ layer is thin enough, typically $\leqslant 3$ u.c.

In the above discussion on $\Delta\sigma$, we have ignored orbital mixing at the $x = 0.4 / x = 0.55$ layer interfaces for the sake of simplicity. In this assumption, conduction electrons in La$_{0.45}$Sr$_{0.55}$MnO$_3$ are two-dimensionally confined in the MnO$_2$ layer at the ground state since the A-type AF spin ordering prohibits carriers hopping along the c direction. When a magnetic field is applied, the AF spin structure in $x = 0.55$ layer is canted to reduce θ from 180°. The reduced θ (and perhaps the associated mixing in of $d_{3z^2-r^2}$ orbital component) induces the c-axis hopping of electrons and resultant dimensional crossover from 2D to 3D. In response to the field-induced deconfinement effect, not only the c-axis resistivity but also the ab plane resistivity should be reduced as a sort of spin-valve effect and this has been observed for the A-type AF state of a Nd$_{1-x}$Sr$_x$MnO$_3$ ($x = 0.55$) crystal.[21] In fact, the MR below T_N, persisting to (or even increasing toward) the lowest temperature, is observed for the present $x = 0.55$ film [see Fig. 1(b)] in contrast to the MR around T_C for the $x = 0.4$ film. Therefore conduction electrons in the FM $x = 0.4$ layers of the superlattice $[F_m, A_n]$ should also be confined within m MnO$_2$ layers without magnetic field because they cannot enter into the AF layers at the interface.

Here we note again that the orbital ordering serves as a driving force for the A-type spin ordering in the $x = 0.55$ layer. If $d_{x^2-y^2}$ electron orbitals in the $x = 0.55$ layer are partially mixed with $d_{x^2-y^2}/d_{3z^2-r^2}$ quantum-disordered orbitals in the $x = 0.4$ layer and possess finite component of $d_{3z^2-r^2}$, the spin angle between neighboring MnO$_2$ atomic layers in the $x = 0.55$ may deviate from 180° as shown in Fig. 11(a). As a result, electron hopping along the c direction in the $x = 0.55$ layer becomes possible as expressed by Eq. (1). This model can explain, beyond the simplest parallel-circuit model, the smaller resistivity of $[F_3, A_3]$ superlattice than that of $[F_{10}, A_{10}]$ superlattice. Further increase of electron hopping between the $x = 0.4$ layers through the $x = 0.55$ intervening layers in the superlattice can be caused by field-induced spin canting in AF layers, as shown in Fig. 11(b). This mechanism should give rise to the effective cou-
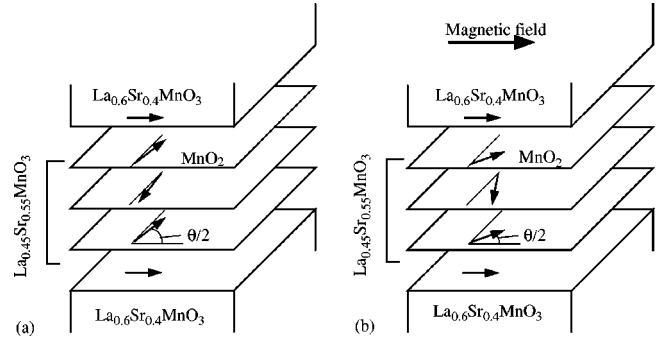

FIG. 11. Schematic illustration of the spin arrangement of the $x = 0.55$ layer in the superlattices. The spin angle between neighboring MnO$_2$ layers in the $x = 0.55$ layer is denoted as θ. (a) θ is deviated from 180° as a result of orbital mixing. (b) A further decrease of θ by field-induced spin canting enhances the possibility of the electron hopping through the $x = 0.55$.

pling between the $x = 0.4$ layers (i.e., dimensional crossover) and the large $\Delta\sigma$ increasing toward low temperature as observed.

IV. SUMMARY

Structural and physical properties of the La$_{1-x}$Sr$_x$MnO$_3$ ($x = 0.4$ and 0.55) single-layer films and the $x = 0.4/x = 0.55$ superlattices were investigated. As in the case of the corresponding bulk crystals, the increase of x from 0.4 to 0.55 alters the metallic ground state of the film from FM to AF (layered or A-type). In particular, strong tensile stress from the SrTiO$_3$ (001) substrate appears to stabilize the $d_{x^2-y^2}$ orbital order for the $x = 0.55$ thin film, and hence the A-type antiferromagnetism. Magnetization and structural characterization of the superlattices indicates that the constituent $x = 0.4$ and $x = 0.55$ layers essentially keep their magnetic properties, even when the constituent $x = 0.4$ layer is as thin as 3 u.c (1.2 nm). Therefore, unlike other superlattices composed of alternate FM and G-type AF layers, the spin ordering at the interface is fairly abrupt on an atomic scale. Overall features of transport properties can be well understood in terms of a simple parallel-circuit model except for the case of the thin ($\leqslant 3$ u.c.) intervening AF film where carrier motion along the c axis becomes possible perhaps via slight modification of the A-type spin ordering. Large $\Delta\sigma$ at low temperatures for such a superlattice film can be interpreted in terms of magnetic-field induced spin canting in the constituent layer, leakage of carriers across the AF layers, and the enhanced coupling between the $x = 0.4$ layers.

[1] For late advance, see, for example, M. Imada, A. Fujimori, and Y. Tokura, Rev. Mod. Phys. **70**, 1218 (1998).

[2] A. Urushibara, Y. Moritomo, T. Arima, A. Asamitsu, G. Kido, and Y. Tokura, Phys. Rev. B **51**, 14 103 (1995).

[3] M. Izumi, Y. Murakami, Y. Konishi, T. Manako, M. Kawasaki, and Y. Tokura, Phys. Rev. B **60**, 1211 (1999).

[4] I. Panagiotopoulos, C. Christides, M. Pissas, and D. Niarchos, Phys. Rev. B **60**, 485 (1999).

[5] H. Tanaka and T. Kawai, Solid State Commun. **112**, 201 (1999).

[6] Y. Tomioka, A. Asamitsu, Y. Moritomo, H. Kuwahara, and Y. Tokura, Phys. Rev. Lett. **74**, 5108 (1995).

[7] H. Kuwahara, Y. Moritomo, Y. Tomioka, A. Asamitsu, M. Kasai, R. Kumai, and Y. Tokura, Phys. Rev. B **56**, 9386 (1997).

[8] H. Fujishiro, M. Ikebe, and Y. Konno, J. Phys. Soc. Jpn. **67**, 1799 (1998).

[9] V. A. Vas'ko, C. A. Nordman, P. A. Kraus, V. S. Achutharaman, A. R. Ruosl, and A. M. Goldman, Appl. Phys. Lett. **68**, 2571 (1996).

[10] J. O'Donnell, M. S. Rzchowski, J. N. Eckstein, and I. Bozovic, Appl. Phys. Lett. **72**, 1775 (1998).

[11] J. M. De Teresa, A. Barthélémy, A. Fert, J. P. Contour, R. Lyonnet, F. Montaigne, P. Seneor, and A. Vaurès, Phys. Rev. Lett. **82**, 4288 (1999).

[12] Y. Suzuki, H. Y. Hwang, S-W. Cheong, and R. B. van Dover, Appl. Phys. Lett. **71**, 140 (1997).

[13] T. K. Nath, R. A. Rao, D. Lavric, C. B. Eom, L. Wu, and F. Tsui, Appl. Phys. Lett. **74**, 1615 (1999).

[14] M. Izumi, Y. Konishi, T. Nishihara, S. Hayashi, M. Shinohara, M. Kawasaki, and Y. Tokura, Appl. Phys. Lett. **73**, 2497 (1998).

[15] H. S. Wang, Q. Li, K. Liu, and C. L. Chien, Appl. Phys. Lett. **74**, 2212 (1999).

[16] W. Prellier, A. Biswas, M. Rajewswari, T. Venkatessan, and R. L. Greene, Appl. Phys. Lett. **75**, 397 (1999).

[17] Y. Konishi, Z. Fang, M. Izumi, T. Manako, M. Kasai, H. Kuwahara, M. Kawasaki, K. Terakura, and Y. Tokura, J. Phys. Soc. Jpn. **68**, 3790 (1999).

[18] M. Kawasaki, M. Izumi, Y. Konishi, T. Manako, and Y. Tokura, Mater. Sci. Eng., B **63**, 49 (1999).

[19] M. Kawasaki, K. Takahashi, T. Maeda, R. Tsuchiya, M. Shinohara, T. Yonezawa, O. Ishihara, M. Yoshimoto, and H. Koinuma, Science **266**, 1540 (1994).

[20] H. Kuwahara, T. Okuda, Y. Tomioka, T. Kimura, A. Asamitsu, and Y. Tokura, in *Science and Technology of Magnetic Oxides*, edited by M. Hundley, J. Nickel, R. Ramesh, and Y. Tokura, MRS Symposia Proceedings No. 494 (Materials Research Society, Pittsburgh, 1998), p. 83.

[21] H. Kuwahara, T. Okuda, Y. Tomioka, A. Asamitsu, and Y. Tokura, Phys. Rev. Lett. **82**, 4316 (1999).

[22] H. Kawano, R. Kajimoto, H. Yoshizawa, Y. Tomioka, H. Kuwahara, and Y. Tokura, Phys. Rev. Lett. **78**, 4253 (1997).

[23] R. Maezono, S. Ishihara, and N. Nagaosa, Phys. Rev. B **57**, R13 993 (1998).

[24] S. Yunoki, A. Moreo, and E. Dagotto, Phys. Rev. Lett. **81**, 5612 (1998).

[25] F. Mack and P. Horsch, Phys. Rev. Lett. **82**, 3160 (1999).

[26] T. Fujiwara and M. Korotin, Phys. Rev. B **59**, 9903 (1999).

[27] J. B. Goodenough, Phys. Rev. **150**, 565 (1955).

[28] Y. Murakami, J. P. Hill, D. Gibbs, M. Blume, I. Koyama, M. Tanaka, H. Kawata, T. Arima, Y. Tokura, K. Hirota, and Y. Endoh, Phys. Rev. Lett. **81**, 582 (1998).

[29] *Metallic Superlattices*, edited by T. Shinjo and T. Takada (Elsevier, Amsterdam, 1987).

[30] *International Tables for Crystallography*, edited by T. Hahn (Kluwer Academic Publishers, Boston, 1995).

[31] A. Berger and H. Hopster, Phys. Rev. Lett. **73**, 193 (1994).

[32] Ernesto J. Escorcia-Aparicio, Hyuk J. Choi, W. L. Ling, R. K. Kawakami, and Z. Q. Qiu, Phys. Rev. Lett. **81**, 2144 (1998).

[33] N. C. Koon, Phys. Rev. Lett. **78**, 4865 (1997).

[34] P. W. Anderson and H. Hasegawa, Phys. Rev. **100**, 675 (1955).